https://doi.org/10.5194/bg-2019-177
Preprint. Discussion started: 3 June 2019

Biogeosciences Discussions

Simulation of factors affecting *E.huxleyi* blooms in arctic and subarctic seas by CMIP5 climate models: model validation and selection

Natalia Gnatiuk[1], Iuliia Radchenko[1], Richard Davy[2], Evgeny Morozov[1], Leonid Bobylev[1]

[1]Nansen International Environmental and Remote Sensing Centre, St. Petersburg, 199034, Russia
[2]Nansen Environmental and Remote Sensing Center, Bergen, N-5006, Norway

Correspondence to: Natalia Gnatiuk (natalia.gnatiuk@niersc.spb.ru)

Abstract. The coccolithophore *E.huxleyi* plays an essential role in the global carbon cycle. Therefore, considering the ongoing global warming, the assessment of future changes in coccolithophore blooms is very important. Our paper aims to provide a framework for selecting the optimum combination of global climate models to conduct such an assessment. To do this we analyse the forcing factors influencing present and future blooms using climate model projections. Then, based on the projected changes in the forcing factors, future changes in the dynamics of coccolithophore *E.huxleyi* blooms can be determined.

Here we describe the complex methodology used for the validation of 34 CMIP5 climate models, and the selection of models that best represent the regional features of the oceanographic and meteorological factors affecting *E.huxleyi* blooms in arctic and subarctic seas: sea surface (i) temperature and (ii) salinity; (iii) wind speed at a height of 10 m above the surface; (iv) ocean surface current speed; and (v) surface downwelling shortwave radiation. The validation of the CMIP5 Atmosphere-Ocean General Circulation Models against reanalysis data includes analysis of the interannual variability, seasonal cycle, spatial biases and temporal trends of the simulated forcing factors. Here we propose a percentile score-based model ranking method for the selection of the best models from the CMIP5 ensemble. The selection of the best models was performed separately for each study area in the Barents, Bering, Greenland, Labrador, North and Norwegian Seas and for each of the five forcing factors affecting the coccolithophore blooms. In total, 30 combinations of most-skilful models were selected. The results show that there is no common optimal combination of models, nor is there one top-model, that has high skill in reproducing regional features across the combination of the five considered forcing factors and all arctic and subarctic seas. However, some climate models consistently show good skill for many of these combinations e.g. ACCESS1-3; ACCESS1-0; HadGEM2-AO; HadGEM2-CC; HadGEM2-ES; GFDL-CM3; INMCM4; GISS-E2-R; GISS-E2-R-CC. The models that have the smallest skill for the majority of the study regions are CMCC-CM; FGOALS-g2; IPSL-CM5A-LR; IPSL-CM5A-MR; IPSL-CM5B-LR; MIROC5; MRI-ESM1.

https://doi.org/10.5194/bg-2019-177
Preprint. Discussion started: 3 June 2019

Biogeosciences Discussions

1 Introduction

The coccolithophores contribute significantly to the global carbon and sulphur cycles (Malin et al., 1993; Matrai et al., 1993; Rivero-Calle et al., 2015; Winter et al., 2013). Additionally, they contribute to the generation of sulfate aerosols which scatter solar radiation in the atmosphere and act as cloud condensation nuclei, enabling cloud formation; therefore, coccolithophores are responsible for both warming and cooling effects on the global climate (Charlson et al., 1987; Wang et al., 2018a, 2018b). Consequently, it is essential to study the dynamics of *E.huxleyi* blooms.

E.huxleyi belongs to the group of small phytoplankton with a size of a few µm, and can form extensive blooms covering more than 100,000 km^2 (Brown and Yoder, 1994; Kondrik et al., 2017; Raitsos et al., 2006). *E.huxleyi* is a temperature and salinity tolerant alga; therefore, it is distributed in the waters of the arctic and subarctic, as well as in equatorial and subtropical waters (Fernandes, 2012; Flores et al., 2010; Kondrik et al., 2017; Okada and McIntyre, 1979; Winter, 1994).

Since changes to the regional climate have influenced the ecosystems of the Arctic seas, coccolithophores, particularly *E.huxleyi*, have increasingly expanded their range into polar waters (Henson et al., 2018; Winter et al., 2013). Winter et al. (2013) suggest that this poleward expansion of *E.huxleyi* is driven by changes in water temperature, salinity, or nutrients. *E.huxleyi* blooms have high positive correlation with the following set of parameters: temperature (3-15 ˚C), high light intensity (25-150 µmol quanta m^2 s^{-1} or 5-33 W m^{-2}) (Iglesias-Rodríguez et al., 2002) and higher N:P ratio (Lavender et al., 2008). Raitsos et al. (2006) noted that the combination of high solar radiation, increased sea surface temperature, and shallow mixed layer depth contributed to the increase in coccolithophores in the North Atlantic region. In addition, wind is one of the environmental factors that influences a bloom of coccolithophores by controlling the amount of vertical mixing in the subsurface layer; therefore, the decrease in wind stress during summer months results in a decrease in the mixed layer depth, and consequently it has a positive effect on *E.huxleyi* growth (Raitsos et al., 2006).

A detailed analysis of a wide range of *forcing factors* (FFs) controlling *E.huxleyi* blooms in arctic and subarctic seas was performed using a machine learning method (Kondrik et al., 2019). Kondrik et al. (2019) identified that sea surface temperature and salinity, near-surface wind speed at a height of 10 m, shortwave downwelling solar radiation, and ocean surface current speed are the most important oceanographic and meteorological factors for the blooming of coccolithophores and ranked the degree of their influence for each of the Barents, Bering, Greenland, Labrador, North and Norwegian Seas. Further, Kondrik et al plan to model the future dynamics of *E.huxleyi* blooms using the statistical models developed in the course of implementing a multifactorial statistical algorithm based on machine learning techniques, described in detail in Kondrik et al. (2019). The model-selection procedure and the resultant optimum combinations of CMIP5 models presented in this paper will be used as input data for Kondrik et al to model the dynamics of blooms in future scenarios. Therefore, the main goal of our study is to validate the ability of CMIP5 climate models to reproduce regional features of the FFs and then to select the best combination of CMIP5 model ensembles to be used in the modelling of the future dynamics of *E.huxleyi* blooms in six arctic and subarctic seas.

https://doi.org/10.5194/bg-2019-177
Preprint. Discussion started: 3 June 2019

It is well established that the ensemble averaging method can be used to reduce the errors, biases and uncertainties in the individual climate models (Flato et al., 2013; Gleckler et al., 2008; Knutti et al., 2010a, 2010b; Pierce et al., 2009; Reichler and Kim, 2008). The main recommendation from climate model developers, in case it is not possible to calibrate a model for a selected region, is to take into consideration more than one climate model (Flato et al., 2013; Gleckler et al., 2008; Knutti et al., 2010b; Pierce et al., 2009). There are two main approaches for the use of climate model ensembles: (i) use of the full-ensemble average data (Flato et al., 2013; Gleckler et al., 2008; Knutti et al., 2010b; Reichler and Kim, 2008); and (ii) selection of an ensemble of the best models from the full set of available climate models (Herger et al., 2018; Knutti et al., 2010b; Taylor, 2001). These two approaches usually give a good result. However, when there are many climate models available (e.g., in our study the number of models available varied from 25 to 30 depending on the climate variable), then the averaging method will result in a very strong smoothing of the data, the interannual variability will be poorly reproduced, and only the long-term trend of a given variable will be well captured. Therefore, we chose the second approach – selection of climate models that properly simulate the regional features (spatial distribution) of the influencing factors under study (sea surface temperature and salinity, surface wind speed at 10 m, ocean surface current speed, and surface downwelling shortwave radiation). At that, it was important to define an appropriate methodology for the selection of the best model ensembles.

There are many approaches for the selection of an optimal set of climate models. One approach suggests choosing models based on the key climatological parameters, e.g., air temperature, precipitation and sea level pressure (Almazroui et al., 2017; Duan and Phillips, 2010; Pierce et al., 2009; Sarr and Sarr, 2017), believing that if the models skillfully reproduce these key parameters, then they also have skill in reproducing the regional climate in general. Another approach which is often used is to select a unique combination of models for each parameter (Agosta et al., 2015; Anav et al., 2013; Fu et al., 2013; Gleckler et al., 2008).

There are many publications which address the selection of climate models, including the application of a ranking method. For example, Agosta et al. (2015) ranked the CMIP5 models using only one statistical metric – a climate prediction index (ratio of root mean square error to standard deviation of observations). Gleckler et al. (2008) evaluated climate models and ranked them analyzing the climatology of the annual cycle, inter-annual variability, and relative errors. They noted that the performance of the climate models varies for different parameters. Das et al. (2018) assessed 34 CMIP5 models using three criteria: mean seasonal cycle, temporal trends, and spatial correlation, and selected the models using a cumulative ranking approach. Fu et al. (2013) and Ruan et al. (2019) applied a score-based method using multiple criteria for the assessment of CMIP5 model performance: mean value, standard deviation, normalized root mean square error, linear correlation coefficient, Mann-Kendall test statistic Z, Sen's slope, and significance score. Further, Ruan et al. (2019) selected the top 25% ranked CMIP5 models for the creation of a multi-model ensemble for air temperature projections over the Lower Mekong Basin. Fu et al. (2013) and Ruan et al. (2019) ranked models using a weight criterion from 0.5 to 1.0. Ruan et al.

https://doi.org/10.5194/bg-2019-177
Preprint. Discussion started: 3 June 2019

(2019) reported that introducing multiple criteria gives less uncertainties in the models' performance in comparison with observation data.

We consider that applying a score-based method using multiple criteria is most appropriate for our study. Since we deal with six arctic and subarctic seas with rather different environmental conditions and a wide range of parameters, it was decided to individually analyze each sea. Moreover, we analyzed the model data only for the areas where *E.huxleyi* blooms were observed to occur, because we highly prioritized the capability of the models to properly capture the local features in the areas of the blooms.

In the following section, we give a description of the data used and methodology applied for the validation analysis and selection of the climate models based on a percentile score-based model ranking for each sea and factor. Section 3 gives a detailed example of the applied methodology and contains results and discussions of the selection of the best climate model ensemble for sea surface temperature in the Barents Sea, along with the overall ranking of models for each considered sea and factor. Analysis of the results from our percentile score-based model ranking method are given in the Supplementary material (spatial distribution of biases and errors in trends for each sea & FF combination). And finally, Section 4 presents the conclusions.

2 Materials and method

2.1 Data

As mentioned above, the FFs influencing the blooms of *E.huxleyi* in arctic and subarctic seas are: sea surface temperature (SST) and salinity averaged over 0-30 m (SSS), surface wind speed at a height of 10 m (WS), ocean surface current speed (OCS), and shortwave downwelling solar radiation (SDSR). For the selection of the best climate models for reproducing the regional features of the distribution of these factors, we used historical projections from Atmosphere-Ocean General Circulation Models (GCMs) that were carried out in the framework of the CMIP5 project, available from the ESGF portal (https://esgf-node.llnl.gov). On the one hand, these models have low resolution (on average it is 150 km), but on the other hand, they include both the atmospheric and oceanic components, and cover all studied regions. Whereas the regional models have high resolution of 11-25 km (e.g., CORDEX) but simulate only atmosphere or ocean separately, and do not cover all six seas within the same model run. In total, we considered 34 GCMs for the historical experiment, but the number of models available for concrete forcing factors varies. The list of climate models used and their main characteristics are presented in Table 1. The atmospheric and oceanic reanalyses data were used for the evaluation and verification of the climate model performance: (i) Era-Interim - for surface wind speed at 10 m, sea surface temperature and shortwave downwelling solar radiation for the period from 1979 to 2005; (ii) GLORYS2V4 - for sea surface salinity and ocean surface current speed for the period from 1993 to 2005. The period for verification of the climate models was chosen based on the length of the reanalysis data and the limitations from the "historical" runs of the climate models, which usually end in 2005.

https://doi.org/10.5194/bg-2019-177
Preprint. Discussion started: 3 June 2019

We used the Era-Interim Reanalysis with the resolution 0.75˚ x 0.75˚ from the European Centre for Medium-Range Weather Forecasts (https://apps.ecmwf.int) (Dee et al., 2011). The GLORYS2V4 (Global Ocean Reanalysis and Simulation version 4) Reanalysis is available at a global scale (with resolution 1˚ x 1˚) from the European Copernicus Marine Environment Monitoring Service (http://marine.copernicus.eu). Selected reanalyses are widely used in the literature and has been shown to be consistent with independent observational data (Agosta et al., 2015; Dee et al., 2011; Garric et al., 2017; Geil et al., 2013).

2.2 Study regions and Methods

Regions under the study are six arctic and subarctic seas: Barents, Bering, Greenland, Labrador, North and Norwegian. The areas where *E.huxleyi* blooms occurred in these regions presented in Fig. 1, showing the number of 8-day periods when blooms were observed. Before conducting a selection of climate models, we applied a spatial-coverage mask to confine the territories of the study seas where blooms occurred more than one 8-day period during 1998-2016. We focused only on the periods of *E.huxleyi* blooms and analysed data for a specific blooming period for each sea with respect to the seasonal distribution of the coccolithophore blooms: June-September for the Barents and Labrador seas, January-December for the Bering Sea, June-August for the Greenland Sea, May-July for the North Sea, and May-August for the Norwegian Sea (Kazakov et al., 2018). Therefore, the selection of the climate models was carried out individually for each sea.

In order to assess how well CMIP5 climate models reproduce regional features of the FFs distribution they were validated by means of comparison of model simulations with the reanalysis data. The methodology of the validation of GCMs included the analysis of the climatological-mean seasonal cycle and interannual variability of FFs for the blooming period in each sea. Seasonal cycle was analysed using multi-year averaged monthly variables for all months of the year (i.e., a sample size of 12), but interannual variability was analysed based on monthly variables for the blooming periods only (sample size varied according to sea and FF combination, e.g., a sample size for SST in the Barents Sea was 108 – monthly variables from June to September during 1979-2005). Basic statistical measures were used for both analyses: correlation coefficient between GCMs and reanalysis (r), root mean square deviation (RMSD), and standard deviation (SD) (Fu et al., 2013; Gleckler et al., 2008; Kumar et al., 2015; Ruan et al., 2019). Additionally, we calculated RMSD-observations standard deviation ratio (RSR) – one of the model evaluation statistics that weighs the simulated data against the observations (Agosta et al., 2015; Golmohammadi et al., 2014; Moriasi et al., 2007; Murphy et al., 2004; Stocker, 2004). For the interannual variability analysis we also calculated the spatial distribution of temporal trends and spatial bias between the model data and reanalysis (Anav et al., 2013; Das et al., 2018; Fu et al., 2013; Gleckler et al., 2008; Kumar et al., 2015; Ruan et al., 2019). Further, we applied our percentile score-based model ranking method of giving a score to each statistical measure for each model. Figure 2 shows an example of this approach applied to RMSD of sea surface temperature in the Barents Sea. We divided the statistical measures into 4 groups based on the amplitude of the calculated metrics and assigned a score to each model according to its group: (i) models considered as very good (less than 25%) were assigned a score of 3; (ii) good models (between 50% and 25%) were assigned a score of 2; (iii) satisfactory models (between 75% and 50%) were assigned a score

https://doi.org/10.5194/bg-2019-177
Preprint. Discussion started: 3 June 2019

of 1; and (iv) unsatisfactory models (more than 75%) were assigned a score of 0. In the case of the correlation coefficient, it is vice versa, very good models with correlations scores above 0.75 ranked with a score of 3, and so forth. Finally, we summed up the total score for each GCM and selected the optimal ensemble of climate models which we take to be the top 25% of GCMs ranked according to their total score. This procedure was applied to each factor and study region.

3 Results and discussion

In this section, we describe the selection of the best GCM ensemble for SST in the Barents Sea as an example of our methodology. In addition, we provide final results of the model ranking – the best model ensembles for each considered factor and sea. The rest of the obtained results are summarised in the supplementary material.

Figure 3 shows two Taylor diagrams, which combine the following statistical measures: correlation coefficient (r), standard deviation (SD) and root-mean-square deviation (RMSD) on one graph and show how well the simulated data fit the observed patterns (Taylor, 2001). Figure 3 illustrates that all GCMs capture the seasonal cycle (left) much better than the interannual variability (right). The obtained correlation coefficient for all models is more than 0.95 for the seasonal cycle, whereas, for the interannual variability it varies from 0.28 to 0.83. Simultaneously, the SD and RMSD have a wide spread of values in both cases – SD for the seasonal cycle varies from 0.27 to 2.67 and for the interannual variability – from 0.75 to 2.55, RMSD ranges from 0.26 to 5.15 for the seasonal cycle and from 0.98 to 7.06 for the interannual variability. The closer the model data to the x-axis, the better the correlation coefficient, and the closer the model data to the dotted line (that represents SD of the reanalysis), the better the model reproduces the variability of the climate parameter. The closer the model data to the reanalysis point, the smaller RMSD that is represented by semicircle lines in Fig. 3. The ranking method was carried out for the correlation coefficient in the range from 0 to 1, where the group with the maximum values in the range 0.75-1 was assigned the score of 3.

Figure 4 presents the box plots of spatial distribution of SST biases in the bloom area of the Barents Sea for the blooming period (June-September) during 1979-2005. For the model ranking, we analysed the absolute values of both median bias and the amplitude of the spatial variation in model biases. The median bias varies from 0 to -6.6 K among the models, whereas the amplitude bias has a wide spread of values from 10.8 to 19.8 K. We can conclude from Fig. 4 that analysis of spatial distribution of biases is very important, e.g., if we compare the model #2 (ACCESS1-3) with the model #3 (CanESM2), we can see that the medians of these two models have small difference (0.28 K), while, the amplitude of spatial values for the model #3 is much higher than for model #2. After the application of the percentile score-based method, the model #2 (ACCESS1-3) was included into the optimal ensemble, whereas and the model #3 (CanESM2) was not included.

Box plots of the spatial distribution of annual trends of SST in the Barents Sea are shown in Fig. 5. The median for SST does not reveal any trend in the Era-Interim reanalysis, while for the models it varies from -0.02 K yr^{-1} to 0.18 K yr^{-1}. From Fig. 5 we can conclude that some models show significant trends. Therefore, if these models show an unrealistic trend during the

https://doi.org/10.5194/bg-2019-177
Preprint. Discussion started: 3 June 2019

historical period, then they could give higher errors in the projections for the future period. For the ranking of models, we analysed the absolute values of differences between model and reanalysis trends, specifically median of the trends and the amplitude of the spatial variation in the trends.

Table 2 presents all calculated statistics that were used to rank GCMs for SST in the Barents Sea as well as the final total score for each model. The spread of the total assigned scores is from 9 to 35. Based on this range we selected the top 25% of GCMs. Thus, the best model ensemble for SST for the Barents Sea is the 8-model set: ACCESS1-0; ACCESS1-3; GFDL-CM3; HadGEM2-AO; HadGEM2-ES; MIROC-ESM; MIROC-ESM-CHEM; MPI-ESM-LR. Additionally, we identified the top-model for SST in this region – MIROC-ESM.

Figure 6 shows the spatial distribution of biases for SST between models and reanalysis in the bloom area in the Barents Sea for the full 28-model ensemble, selected 8-model ensemble, and top-model. As we can see, the full 28-model set underestimates the SST in the study region while the top-model, MIROC-ESM, overestimates it. The selected 8-model ensemble shows smaller biases (± 1 K) in SST for the majority of the bloom area in the Barents Sea.

The spatial distribution of errors in SST trends between models and reanalysis in the study region is presented in Fig. 7. The full 28-model ensemble overestimates trends for the whole study region (model-reanalysis errors are 0.03-0.07 K yr^{-1}), the top-model MIROC-ESM partly underestimates the SST trend, but mainly reveals similar to Era-Interim reanalysis insignificant trends (± 0.01 K yr^{-1}). As for the selected 8-model ensemble, the spatial variability of errors in trends for SST varies from -0.01 to 0.06 K yr^{-1}, although for the major part of the study region the errors are -0.01 to 0.02 K yr^{-1}.

SST variability and spatially-averaged annual trends are presented in Fig. 8. As we can see, the full 28-model ensemble notably underestimates the interannual variability of SST and shows a significant positive trend (0.04 K yr^{-1} – statistically significant at the level of $p < 0.05$), while the top-model MIROC-ESM overestimates SST and shows a non-significant negative trend (-0.005 K yr^{-1}). The optimal 8-model ensemble has better performance in the SST, even though it shows a slight positive trend (0.02 K yr^{-1} – statistically significant at the level of $p < 0.05$) compared with a non-significant trend in the Era-Interim reanalysis– (0.002 K yr^{-1}).

The selected optimal CMIP5 model ensembles for the other seas and FFs are presented in Fig. 9. The heat map shows the final model scores, which represent the results of our percentile score-based model ranking approach. The map summarises scores for five FFs that influence blooms of *E.huxleyi* (OCS, SSS, SST, WS, and SDSR) in six arctic and subarctic seas (Barents, Bering, Greenland, Labrador, North, and Norwegian). The top 25% of GCMs were selected as the optimal model ensemble for each sea and forcing factor combination (total 30 model ensembles: six seas multiplied by five factors). From the heat map we can conclude, that there is no optimal model ensemble, or one top-model, which could properly simulate all factors over all study regions. However, some climate models show good results for many cases, e.g., ACCESS1-3; ACCESS1-0; HadGEM2-AO; HadGEM2-CC; HadGEM2-ES; GFDL-CM3; INMCM4; GISS-E2-R; GISS-E2-R-CC. The model that have higher biases across the majority of the study regions are CMCC-CM; FGOALS-g2; IPSL-CM5A-LR; IPSL-CM5A-MR; IPSL-CM5B-LR; MIROC5; MRI-ESM1.

https://doi.org/10.5194/bg-2019-177
Preprint. Discussion started: 3 June 2019

To examine our percentile score-based model ranking method we analysed the spatial distribution of biases and errors in trends for the full-model ensemble, selected best-model ensemble, and top-model vs. reanalysis data for each sea & FF combination (see Supplements). In general, the selected best-model ensemble shows better performance than either the full-model ensemble or the single top-model. The selected best-model ensembles are better in 74% and 83%, equal in 13% and 10% and worse in 13% and 7% of cases than the full-model ensemble or/and top-model for biases and trends respectively.

4 Conclusions

A percentile score-based model ranking method has been presented for the selection of the optimal model ensembles, from a total of 34 CMIP5 models, for five different climate variables that have previously been identified as influencing *E.huxleyi* blooms (SST, WS, SSS, OCS, SDSR) in six arctic and subarctic seas (Barents, Bering, Labrador, Greenland, North, Norwegian). The optimal ensembles for each factor and each sea were selected (in total 30 combinations of most-skilful models) based on different statistical measures: root mean square error, correlation coefficient, standard deviation, RMSD-observations standard deviation ratio, spatial biases and trends. Our results show that there is no optimal model ensemble or one top-model which could best simulate all factors across all of the study regions. Despite the fact that the Arctic is often considered as one single region in many studies, our results show that CMIP5 climate models do not have consistent performance across such a large area. However, the selected optimal model ensembles show quite good results with lesser biases in smaller study regions, i.e., individual Arctic seas.

Since we plan to apply CMIP5 model projections for the modelling of the dynamics of *E.huxleyi* blooms in the future, it is essential to select climate models that properly simulate the spatial distribution of the FFs. Therefore, we suppose that the spatial distribution of biases and trends in FFs are more important in the model selection procedure. From our results we can also conclude that it is essential to not only analyse spatially averaged values, but also the amplitude of the spatial distribution.

The results of examining of our percentile score-based model ranking method proposed in the paper generally show better performance of selected model ensemble vs. full-model ensemble or single best-model for different variables and regions. Due to the short sample period of reanalysis data (1979-2005), we did this evaluation without out-of-sample testing. Definitely, it is better to test any model ranking method on another historical period. It will be possible to consider the period 1950-2014 with the release of new data, e.g., CMIP6, ERA5.

We can conclude that a range of different factors are important, including the spatial pattern of model biases, and that proposed methodology is one way we could increase the sophistication of model selection procedures to give us a better chance at selecting more skillful models for those features in which we are interested. Thus, the proposed method can be applied for the analysis in other regions to evaluate climate model performance for various atmospheric and oceanic parameters at regional scales.

https://doi.org/10.5194/bg-2019-177
Preprint. Discussion started: 3 June 2019

Author contribution

NG, RD, LB: methodology development. NG, IR: development of the paper concept. IR, NG, EM: data processing and figures producing. All authors contributed to the writing and discussion of the manuscript.

Competing interests

The authors declare that they have no conflict of interest.

Acknowledgements

We express our gratitude for the financial support of this study provided by the Russian Science Foundation (RSF) under the project 17-17-01117.

N. Gnatiuk and I. Radchenko gratitude Dmitry Pozdnyakov for the invitation to participate in the project and thank him and Dmitry Kondrik for discussion of the manuscript.

We acknowledge the members of the Coupled Model Intercomparison Project phase 5, the European Centre for Medium-Range Weather Forecasts, the European Copernicus Marine Environment Monitoring Service, and we gratitude the modelling groups (mentioned in Table 1).

https://doi.org/10.5194/bg-2019-177
Preprint. Discussion started: 3 June 2019

References

Agosta, C., Fettweis, X. and Datta, R.: Evaluation of the CMIP5 models in the aim of regional modelling of the Antarctic surface mass balance, Cryosph., 9, 2311–2321, 2015.

Almazroui, M., Nazrul Islam, M., Saeed, S., Alkhalaf, A. K. and Dambul, R.: Assessment of Uncertainties in Projected Temperature and Precipitation over the Arabian Peninsula Using Three Categories of Cmip5 Multimodel Ensembles, Earth Syst. Environ., 1(2), 23, doi:10.1007/s41748-017-0027-5, 2017.

Anav, A., Friedlingstein, P., Kidston, M., Bopp, L., Ciais, P., Cox, P., Jones, C., Jung, M., Myneni, R. and Zhu, Z.: Evaluating the Land and Ocean Components of the Global Carbon Cycle in the CMIP5 Earth System Models, J. Clim., 26(18), 6801–6843, doi:10.1175/JCLI-D-12-00417.1, 2013.

Brown, C. W. and Yoder, J. A.: Coccolithophorid blooms in the global ocean, J. Geophys. Res., 99(C4), 7467, doi:10.1029/93JC02156, 1994.

Charlson, R. J., Lovelock, J. E., Andreae, M. O. and Warren, S. G.: Oceanic phytoplankton, atmospheric sulphur, cloud albedo and climate, Nature, 326, 655–661, 1987.

Das, L., Dutta, M., Mezghani, A. and Benestad, R. E.: Use of observed temperature statistics in ranking CMIP5 model performance over the Western Himalayan Region of India, Int. J. Climatol., 38(2), 554–570, doi:10.1002/joc.5193, 2018.

Dee, D. P., Uppala, S. M., Simmons, A. J., Berrisford, P., Poli, P., Kobayashi, S., Andrae, U., Balmaseda, M. A., Balsamo, G., Bauer, P., Bechtold, P., Beljaars, A. C. M., van de Berg, L., Bidlot, J., Bormann, N., Delsol, C., Dragani, R., Fuentes, M., Geer, A. J., Haimberger, L., Healy, S. B., Hersbach, H., Hólm, E. V., Isaksen, L., Kållberg, P., Köhler, M., Matricardi, M., McNally, A. P., Monge-Sanz, B. M., Morcrette, J.-J., Park, B.-K., Peubey, C., de Rosnay, P., Tavolato, C., Thépaut, J.-N. and Vitart, F.: The ERA-Interim reanalysis: configuration and performance of the data assimilation system, Q. J. R. Meteorol. Soc., 137(656), 553–597, doi:10.1002/qj.828, 2011.

Duan, Q. and Phillips, T. J.: Bayesian estimation of local signal and noise in multimodel simulations of climate change, J. Geophys. Res., 115(D18), D18123, doi:10.1029/2009JD013654, 2010.

Fernandes, M.: The Influence of Stress Conditions on Intracellular Dimethylsulphoniopropionate (DMSP) and Dimethylsulphide (DMS) Release in Emiliania huxleyi., 2012.

Flato, G., Marotzke, J., Abiodun, B., Braconnot, P., Chou, S. C., Collins, W., Cox, P., Driouech, F., Emori, S., Eyring, V., Forest, C., Gleckler, P., Guilyardi, E., Jakob, C., Kattsov, V., Reason, C. and Rummukainen, M.: Evaluation of Climate Models, in Climate Change 2013: The Physical Science Basis. Contribution of Working Group I to the Fifth Assess- ment Report of the Intergovernmental Panel on Climate Change, pp. 741–866, NY., 2013.

Flores, J. A., Colmenero-Hidalgo, E., Mejía-Molina, A. E., Baumann, K. H., H., J., L. and Rodrigues, T.: Distribution of large Emiliania huxleyi in the Central and Northeast Atlantic as a tracer of surface ocean dynamics during the last 25,000 years, Mar. Micropaleontol., 76, 53–66, 2010.

Fu, G., Liu, Z., Charles, S. P., Xu, Z. and Yao, Z.: A score-based method for assessing the performance of GCMs: A case study of southeastern Australia, J. Geophys. Res. Atmos., 118(10), 4154–4167, doi:10.1002/jgrd.50269, 2013.

Garric, G., Parent, L., Greiner, E., Drévillon, M., Hamon, M., Lellouche, J.-M., Régnier, C., Desportes, C., Le Galloudec, O., Bricaud, C., Drillet, Y., Hernandez, F. and Le Traon, P.-Y.: Performance and quality assessment of the global ocean eddy-permitting physical reanalysis GLORYS2V4., 19th EGU Gen. Assem. EGU2017, Proc. from Conf. held 23-28 April. 2017 Vienna, Austria., p.18776, 19, 18776, 2017.

Geil, K. L., Serra, Y. L., Zeng, X., Geil, K. L., Serra, Y. L. and Zeng, X.: Assessment of CMIP5 Model Simulations of the North American Monsoon System, J. Clim., 26(22), 8787–8801, doi:10.1175/JCLI-D-13-00044.1, 2013.

Gleckler, P. J., Taylor, K. E. and Doutriaux, C.: Performance metrics for climate models, J. Geophys. Res. Atmos., 113(D6),

https://doi.org/10.5194/bg-2019-177
Preprint. Discussion started: 3 June 2019

D06104, doi:10.1029/2007JD008972, 2008.

Golmohammadi, G., Prasher, S., Madani, A. and Rudra, R.: Evaluating Three Hydrological Distributed Watershed Models: MIKE-SHE, APEX, SWAT, Hydrology, 1(1), 20–39, doi:10.3390/hydrology1010020, 2014.

Henson, S. A., Cole, H. S., Hopkins, J., Martin, A. P. and Yool, A.: Detection of climate change-driven trends in phytoplankton phenology, Glob. Chang. Biol., 24(1), e101–e111, doi:10.1111/gcb.13886, 2018.

Herger, N., Abramowitz, G., Knutti, R., Angélil, O., Lehmann, K. and Sanderson, B. M.: Selecting a climate model subset to optimise key ensemble properties, Earth Syst. Dyn., 9(1), 135–151, doi:10.3929/ETHZ-B-000246202, 2018.

Iglesias-Rodríguez, M. D., Brown, C. W., Doney, S. C., Kleypas, J., Kolber, D., Kolber, Z., Hayes, P. K. and Falkowski, P. G.: Representing key phytoplankton functional groups in ocean carbon cycle models: Coccolithophorids, Global Biogeochem. Cycles, 16(4), 47-1-47–20, doi:10.1029/2001GB001454, 2002.

Kazakov, E., Kondrik, D. and Pozdnyakov, D.: Spatial data assimilation with a service-based GIS infrastructure for mapping and analysis of E. Huxleyi blooms in arctic seas, in Sixth International Conference on Remote Sensing and Geoinformation of the Environment., 2018.

Knutti, R., Furrer, R., Tebaldi, C., Cermak, J., Meehl, G. A., Knutti, R., Furrer, R., Tebaldi, C., Cermak, J. and Meehl, G. A.: Challenges in Combining Projections from Multiple Climate Models, J. Clim., 23(10), 2739–2758, doi:10.1175/2009JCLI3361.1, 2010a.

Knutti, R., Abramowitz, G., Collins, M., Eyring, V., Gleckler, P. J., Hewitson, B. and Mearns, L.: Good practice guidance paper on assessing and combining multi model climate projections., 2010b.

Kondrik, D., Pozdnyakov, D. and Pettersson, L.: Particulate inorganic carbon production within E. huxleyi blooms in subpolar and polar seas: a satellite time series study (1998–2013), Int. J. Remote Sens., 38(22), 6179–6205, doi:10.1080/01431161.2017.1350304, 2017.

Kondrik, D., Kazakov, E., Chepikova, S. and Pozdnyakov, D.: Prioritization of the vector factors controlling Emiliania huxleyi blooms in subarctic and arctic seas: A multidimensional statistical approach, Biogeosciences Discuss., 1–24, doi:10.5194/bg-2019-104, 2019.

Kumar, D., Mishra, V. and Ganguly, A. R.: Evaluating wind extremes in CMIP5 climate models, Clim. Dyn., 45(1–2), 441–453, doi:10.1007/s00382-014-2306-2, 2015.

Lavender, S. J., Raitsos, D. E. and Pradhan, Y.: Variations in the Phytoplankton of the North-Eastern Atlantic Ocean: From the Irish Sea to the Bay of Biscay, in Remote Sensing of the European Seas, pp. 67–78, Springer Netherlands, Dordrecht., 2008.

Malin, G., Turner, S., Liss, P., Holligan, P. and Harbour, D.: Dimethylsulphide and dimethylsulphoniopropionate in the Northeast atlantic during the summer coccolithophore bloom, Deep Sea Res. Part I Oceanogr. Res. Pap., 40(7), 1487–1508, doi:10.1016/0967-0637(93)90125-M, 1993.

Matrai, P. A. and Keller, M. D.: Dimethylsulfide in a large-scale coccolithophore bloom in the Gulf of Maine, Cont. Shelf Res., 13(8–9), 831–843, 1993.

Moriasi, D. N., Arnold, J. G., Liew, M. W. Van, Bingner, R. L., Harmel, R. D. and Veith, T. L.: Model evaluation guidelines for systematic quantification of accuracy in watershed simulations, Am. Soc. Agric. Biol. Eng., 50(3), 885–900, 2007.

Murphy, J. M., Sexton, D. M. H., Barnett, D. N., Jones, G. S., Webb, M. J., Collins, M. and Stainforth, D. A.: Quantification of modelling uncertainties in a large ensemble of climate change simulations, Nature, 430(7001), 768–772, doi:10.1038/nature02771, 2004.

Okada, H. and McIntyre, A.: Seasonal distribution of modern coccolithophores in the western North Atlantic Ocean, Mar. Biol., 54(4), 319–328, doi:10.1007/BF00395438, 1979.

Pierce, D. W., Barnett, T. P., Santer, B. D. and Gleckler, P. J.: Selecting global climate models for regional climate change studies, Proc. Natl. Acad. Sci., 106(21), 8441–8446, 2009.

Raitsos, D. E., Lavender, S. J., Pradhan, Y., Tyrrell, T., Reid, P. C. and Edwards, M.: Coccolithophore bloom size variation in response to the regional environment of the subarctic North Atlantic, Limnol. Oceanogr., 51(5), 2122–2130, doi:10.4319/lo.2006.51.5.2122, 2006.

Reichler, T. and Kim, J.: How Well Do Coupled Models Simulate Today's Climate?, Bull. Am. Meteorol. Soc., 89(3), 303–312, doi:10.1175/BAMS-89-3-303, 2008.

Rivero-Calle, S., Gnanadesikan, A., Castillo, C. E. Del, Balch, W. M. and Guikema, S. D.: Multidecadal increase in North Atlantic coccolithophores and the potential role of rising CO2, Science (80-.)., 350(6267), 2015.

Ruan, Y., Liu, Z., Wang, R. and Yao, Z.: Assessing the Performance of CMIP5 GCMs for Projection of Future Temperature Change over the Lower Mekong Basin, Atmosphere (Basel)., 10(2), 93, doi:10.3390/atmos10020093, 2019.

Sarr, A. and Sarr, A.: Multi-Scale Characteristics of Precipitation and Temperature over West Africa Using SMHI-RCA Driven by GCMs under RCP8.5, Am. J. Clim. Chang., 06(03), 455–486, doi:10.4236/ajcc.2017.63024, 2017.

Stocker, T. F.: Models change their tune, Nature, 430(7001), 737–738, doi:10.1038/430737a, 2004.

Taylor, K. E.: Summarizing multiple aspects of model performance in a single diagram, J. Geophys. Res. Atmos., 106(D7), 7183–7192, doi:10.1029/2000JD900719, 2001.

Wang, S., Maltrud, M. E., Burrows, S. M., Elliott, S. M. and Cameron-Smith, P.: Impacts of Shifts in Phytoplankton Community on Clouds and Climate via the Sulfur Cycle, Global Biogeochem. Cycles, 32(6), 1005–1026, doi:10.1029/2017GB005862, 2018a.

Wang, S., Maltrud, M., Elliott, S., Cameron-Smith, P. and Jonko, A.: Influence of dimethyl sulfide on the carbon cycle and biological production, Biogeochemistry, 138(1), 49–68, doi:10.1007/s10533-018-0430-5, 2018b.

Winter, A.: Biogeography of living coccolithophores in ocean waters, Coccolithophores, 1994.

Winter, A., Henderiks, J., Beaufort, L., Rickaby, R. E. M. and Brown, C. W.: Poleward expansion of the coccolithophore Emiliania huxleyi, J. Plankton Res., 36(2), 316–325, doi:10.1093/plankt/fbt110, 2013.

https://doi.org/10.5194/bg-2019-177
Preprint. Discussion started: 3 June 2019

Biogeosciences Discussions Open Access EGU

Table 1. CMIP5 models used for simulation of forcing factors influencing E.huxleyi blooms (models available for concrete factor are marked as "+")

Model	**ID**	**Modelling Center** (acronym, full name, and country)	**Resolution** (°lon x °lat)	**SST**	**WS**	**SDSR**	**SSS**	**OCS**
ACCESS1.0	1	CSIRO-BOM, Commonwealth Scientific and Industrial Research Organisation, Australia and Bureau of Meteorology, Australia	1.25 x 1.875	+	+	+	+	+
ACCESS1.3	2			+	+	+	+	+
CanESM2	3	CCCma, Canadian Centre for Climate Modelling and Analysis, Canada	2.7906 x 2.8125	+	+		+	+
CMCC-CM	4	CMCC, Centro euro-Mediterraneo sui Cambiamenti Climatici, Italy	0.7484 x 0.75	+	+	+	+	+
CMCC-CMS	5		3.7111 x 3.75	+	+	+	+	+
CNRM-CM5	6	CNRM-CERFACS, Centre National de Recherches Meteorologiques, France and Centre Europeen de Recherche et Formation Avancees en Calcul Scientifique, France	1.4008 x 1.40625	+	+	+	+	+
CSIRO-Mk3.6.0	7	CSIRO-QCCCE, Commonwealth Scientific and Industrial Research Organization, Australia and Queensland Climate Change Centre of Excellence, Australia	1.8653 x 1.875		+	+	+	+
EC-EARTH	8	EC-EARTH, EC-EARTH consortium, Europe	1.1215 x 1.125	+				
GFDL-CM3	9	NOAA GFDL, National Oceanic and Atmospheric Administration, Geophysical Fluid Dynamics Laboratory, USA	2 x 2.5	+	+	+	+	+
GFDL-ESM2G	10			+	+	+	+	+
GFDL-ESM2M	11			+	+	+	+	+
GISS-E2-H	12	NASA GISS, National Aeronautics and Space Administration, Goddard Institute for Space Studies, USA	2 x 2.5	+	+	+	+	+
GISS-E2-H-CC	13			+	+	+	+	+
GISS-E2-R	14			+	+	+	+	+
GISS-E2-R-CC	15			+	+	+	+	+
HadCM3	16	MOHC INPE, Met Office Hadley Centre, UK and Instituto Nacional de Pesquisas Espaciais, Brasil	2.5 x 3.75		+			
HadGEM2-AO	17		1.25 x 1.875	+	+	+	+	+
HadGEM2-CC	18			+	+	+	+	+
HadGEM2-ES	19			+	+	+	+	+
IPSL-CM5A-LR	20	IPSL, Institut Pierre-Simon Laplace, France	1.8947 x 3.75	+	+	+	+	+

https://doi.org/10.5194/bg-2019-177
Preprint. Discussion started: 3 June 2019

IPSL-CM5A-MR	21			+	+	+	+	+
IPSL-CM5B-LR	22			+	+	+	+	+
MIROC5	23	MIROC, Atmosphere and Ocean Research Institute, the University of Tokyo, National Institute for Environmental Studies, and Japan Agency for Marine-Earth Science and Technology, Japan	1.4008 x 1.40625	+	+	+	+	
MIROC4h	24		0.5616 x 0.5625		+			
MIROC-ESM	25	MIROC, Japan Agency for Marine-Earth Science and Technology, Atmosphere and Ocean Research Institute, the University of Tokyo, and National Institute for Environmental Studies, Japan	2.7906 x 2.8125	+	+	+	+	
MIROC-ESM-CHEM	26			+	+	+	+	
MPI-ESM-LR	27	MPI-M, Max Planck Institute for Meteorology, Germany	1.8653 x 1.875	+	+	+	+	+
MPI-ESM-MR	28			+	+	+	+	+
MRI-CGCM3	29	MRI, Meteorological Research Institute, Japan	1.12148 x 1.125	+	+	+	+	+
MRI-ESM1	30				+			
NorESM1-M	31	NCC, Norwegian Climate Centre, Norway	1.8947 x 2.5	+		+	+	
NorESM1-ME	32			+		+	+	+
INM-CM4	33	INM, Russian Academy of Sciences Marchuk Institute of Numerical Mathematics, Russia	1.5 x 2		+	+		
FGOALS-g2	34	LASG-CESS, Institute of Atmospheric Physics, Chinese Academy of Sciences; and Tsinghua University, China	2.7906 x 2.8125					+

https://doi.org/10.5194/bg-2019-177
Preprint. Discussion started: 3 June 2019

Biogeosciences Discussions Open Access EGU

Table 2. Results of the CMIP5 model performance for SST in the Barents Sea.

(Numbers in brackets indicate the models scores. RMSD - root-mean-square deviation; r – correlation coefficient between models and reanalysis; RSR – RMSD-observations standard deviation ratio; |SDdif| – modulus of standard deviation difference (model minus reanalysis); |Trm| - modulus of spatial trend median difference (model minus reanalysis); |Tra| - modulus of spatial trend amplitude difference (model minus reanalysis); |Brm| - modulus of spatial trend median difference (model minus reanalysis); |Bra| – modulus of spatial biases amplitude difference (model minus reanalysis)).

Model acronym	ID	Interannual variability (averaged over the territory)				Seasonal cycle (averaged over the territory)				Spatial trends (Tr) and biases (Br)				Total score
		RMSD	r	RSR	$\|SD_{dif}\|$	RMSD	r	RSR	$\|SD_{dif}\|$	$\|Tr_m\|$	$\|Tr_a\|$	$\|Br_m\|$	$\|Br_a\|$	
ACCESS1-0	1	0,26*(3)*	0,99*(2)*	0,13*(3)*	0,08*(3)*	1,17*(3)*	0,68*(3)*	0,81*(3)*	0,02*(3)*	0,06*(2)*	0,01*(3)*	0,07(3)	14,7(2)	**33**
ACCESS1-3	2	0,37*(3)*	0,99*(3)*	0,19*(3)*	0,03*(3)*	1,02*(3)*	0,75*(3)*	0,71*(3)*	0,19*(3)*	0,01*(3)*	0,01*(3)*	0,57*(3)*	16,1*(1)*	**34**
CanESM2	3	1,76*(2)*	0,98*(2)*	0,88*(2)*	0,28*(0)*	2,21*(2)*	0,64*(3)*	1,54*(2)*	1,12*(3)*	0,10*(1)*	0,04*(3)*	0,85*(3)*	17,2*(1)*	24
CMCC-CM	4	5,15*(0)*	0,96*(1)*	2,58*(0)*	1,73*(1)*	7,06*(0)*	0,28*(3)*	4,90*(0)*	0,63*(0)*	0,06*(2)*	0,18*(0)*	6,64*(0)*	13,1*(2)*	9
CMCC-CMS	5	4,40*(0)*	0,97*(2)*	2,20*(0)*	1,34*(1)*	5,94*(0)*	0,56*(3)*	4,12*(0)*	0,59*(0)*	0,01*(3)*	0,02*(3)*	5,58*(0)*	14,1*(2)*	14
CNRM-CM5	6	0,64*(3)*	0,99*(2)*	0,32*(3)*	0,55*(1)*	1,59*(3)*	0,73*(3)*	1,10*(3)*	0,81*(2)*	0,08*(2)*	0,00*(3)*	0,49*(3)*	16,4*(1)*	29
EC-EARTH	7	0,41*(3)*	0,99*(2)*	0,21*(3)*	0,13*(2)*	1,43*(3)*	0,64*(3)*	0,99*(3)*	0,38*(3)*	0,13*(1)*	0,12*(1)*	0,14*(3)*	18,1*(0)*	27
GFDL-CM3	8	1,34*(3)*	0,99*(3)*	0,67*(3)*	0,20*(3)*	1,71*(3)*	0,80*(3)*	1,19*(3)*	0,22*(3)*	0,00*(3)*	0,09*(1)*	1,39*(3)*	11,1*(3)*	**34**
GFDL-ESM2G	9	3,23*(1)*	0,98*(2)*	1,62*(1)*	0,27*(2)*	3,72*(1)*	0,69*(3)*	2,58*(1)*	0,29*(3)*	0,04*(3)*	0,04*(3)*	3,46*(1)*	13,9*(2)*	23
GFDL-ESM2M	10	2,60*(2)*	0,99*(2)*	1,30*(2)*	0,61*(3)*	3,42*(2)*	0,68*(3)*	2,37*(2)*	0,25*(2)*	0,01*(3)*	0,08*(2)*	3,10*(2)*	15,7*(1)*	26
GISS-E2-H	11	3,39*(1)*	0,97*(3)*	1,70*(1)*	0,41*(3)*	4,09*(1)*	0,83*(3)*	2,84*(1)*	0,18*(3)*	0,05*(2)*	0,04*(3)*	3,86*(1)*	11,4*(3)*	25
GISS-E2-H-CC	12	3,68*(1)*	0,96*(2)*	1,84*(1)*	0,56*(3)*	4,62*(1)*	0,72*(3)*	3,20*(1)*	0,12*(2)*	0,03*(3)*	0,02*(3)*	4,36*(1)*	10,8*(3)*	24
GISS-E2-R	13	3,34*(1)*	0,96*(2)*	1,67*(1)*	0,04*(1)*	3,83*(1)*	0,72*(3)*	2,66*(1)*	0,84*(3)*	0,05*(2)*	0,07*(2)*	3,34*(1)*	15,1*(2)*	20
GISS-E2-R-CC	14	3,38*(1)*	0,96*(2)*	1,69*(1)*	0,07*(1)*	3,78*(1)*	0,75*(3)*	2,62*(1)*	0,83*(3)*	0,03*(3)*	0,05*(2)*	3,29*(2)*	13,6*(2)*	22
HadGEM2-AO	15	1,28*(3)*	0,99*(2)*	0,64*(3)*	0,01*(3)*	1,51*(3)*	0,73*(3)*	1,05*(3)*	0,13*(3)*	0,02*(3)*	0,05*(2)*	1,33*(3)*	19,8*(0)*	31
HadGEM2-CC	16	1,70*(2)*	0,99*(2)*	0,85*(2)*	0,16*(2)*	2,34*(2)*	0,62*(3)*	1,62*(2)*	0,35*(3)*	0,05*(2)*	0,05*(2)*	1,66*(3)*	19,1*(0)*	25
HadGEM2-ES	17	0,30*(3)*	0,99*(3)*	0,15*(3)*	0,08*(3)*	0,98*(3)*	0,77*(3)*	0,68*(3)*	0,00*(3)*	0,05*(2)*	0,04*(3)*	0,09*(3)*	17,5*(1)*	**33**
IPSL-CM5A-LR	18	3,66*(1)*	0,98*(2)*	1,83*(1)*	0,31*(3)*	4,59*(1)*	0,70*(3)*	3,19*(1)*	0,18*(3)*	0,01*(3)*	0,03*(3)*	4,32*(1)*	18,4*(0)*	22
IPSL-CM5A-MR	19	2,22*(2)*	0,99*(2)*	1,11*(2)*	0,67*(1)*	2,57*(2)*	0,73*(3)*	1,78*(2)*	0,80*(2)*	0,06*(2)*	0,05*(2)*	1,91*(2)*	16,0*(1)*	23
IPSL-CM5B-LR	20	5,03*(0)*	0,96*(1)*	2,52*(0)*	1,71*(1)*	6,90*(0)*	0,36*(3)*	4,79*(0)*	0,69*(0)*	0,00*(3)*	0,03*(3)*	6,51*(0)*	17,6*(0)*	11
MIROC-ESM	21	1,40*(3)*	0,99*(3)*	0,70*(3)*	0,04*(3)*	1,63*(3)*	0,82*(3)*	1,13*(3)*	0,06*(3)*	0,01*(3)*	0,08*(2)*	1,51*(3)*	11,8*(3)*	**35**
MIROC-ESM-CHEM	22	0,97*(3)*	0,99*(3)*	0,49*(3)*	0,05*(3)*	1,34*(3)*	0,82*(3)*	0,93*(3)*	0,13*(3)*	0,07*(2)*	0,05*(3)*	1,08*(3)*	15,1*(2)*	**34**
MIROC5	23	2,42*(0)*	0,98*(2)*	1,21*(0)*	0,51*(1)*	5,69*(2)*	0,51*(3)*	3,95*(2)*	0,64*(2)*	0,18*(0)*	0,08*(2)*	5,14*(0)*	19,8*(0)*	14
MPI-ESM-LR	24	1,27*(3)*	0,99*(3)*	0,63*(3)*	0,04*(3)*	1,54*(3)*	0,81*(3)*	1,07*(3)*	0,21*(3)*	0,02*(3)*	0,04*(3)*	1,33*(3)*	16,3*(1)*	**34**
MPI-ESM-MR	25	0,91*(3)*	0,99*(2)*	0,45*(3)*	0,05*(3)*	1,47*(3)*	0,71*(3)*	1,02*(3)*	0,11*(3)*	0,05*(2)*	0,04*(3)*	0,96*(3)*	17,2*(1)*	**32**
MRI-CGCM3	26	2,88*(2)*	0,99*(3)*	1,44*(2)*	0,08*(2)*	2,54*(1)*	0,82*(3)*	1,77*(1)*	0,34*(3)*	0,00*(3)*	0,07*(2)*	2,30*(2)*	11,9*(3)*	27
NorESM1-M	27	1,53*(2)*	0,99*(2)*	0,77*(2)*	0,76*(2)*	2,56*(2)*	0,64*(3)*	1,78*(2)*	0,31*(2)*	0,05*(2)*	0,07*(2)*	2,33*(2)*	13,7*(2)*	25
NorESM1-ME	28	1,72*(2)*	0,99*(2)*	0,86*(2)*	0,78*(2)*	2,79*(2)*	0,57*(3)*	1,94*(2)*	0,39*(2)*	0,02*(3)*	0,02*(3)*	2,58*(2)*	15,0*(2)*	27

https://doi.org/10.5194/bg-2019-177
Preprint. Discussion started: 3 June 2019

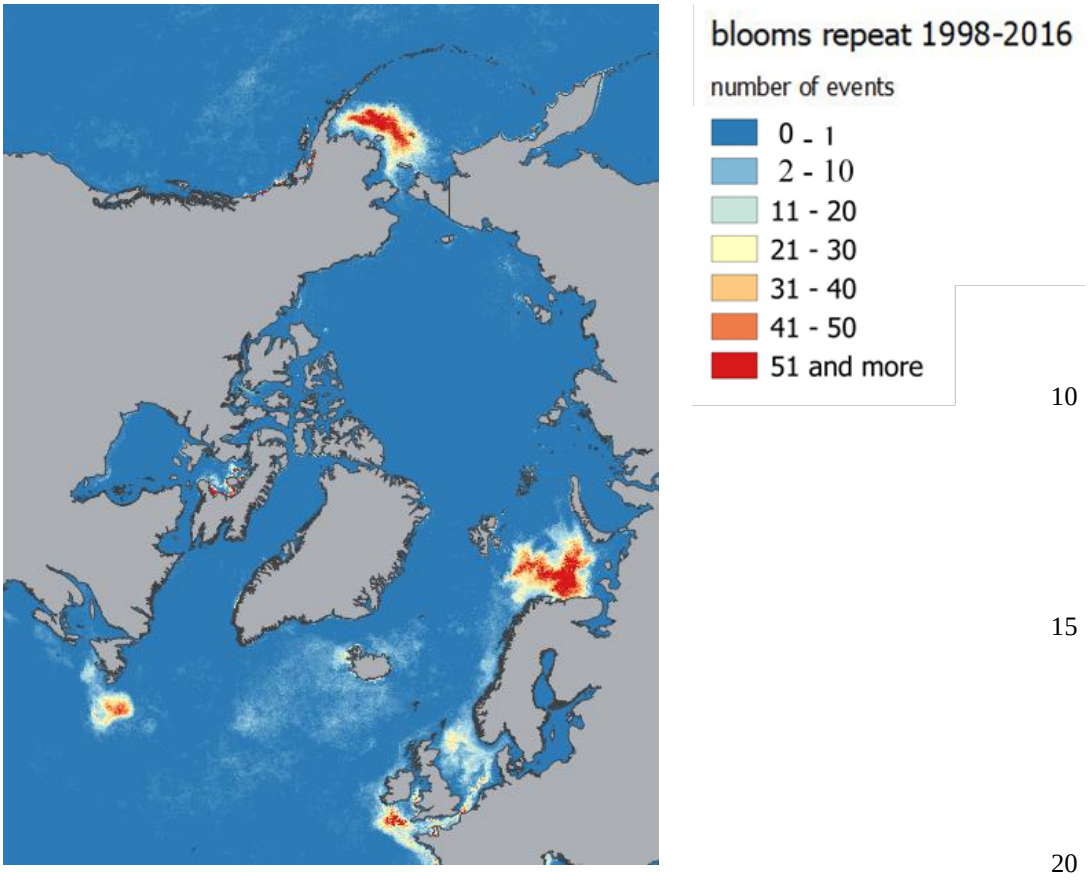

Figure 1: Location of the E.huxleyi blooming areas in the study regions.

https://doi.org/10.5194/bg-2019-177
Preprint. Discussion started: 3 June 2019

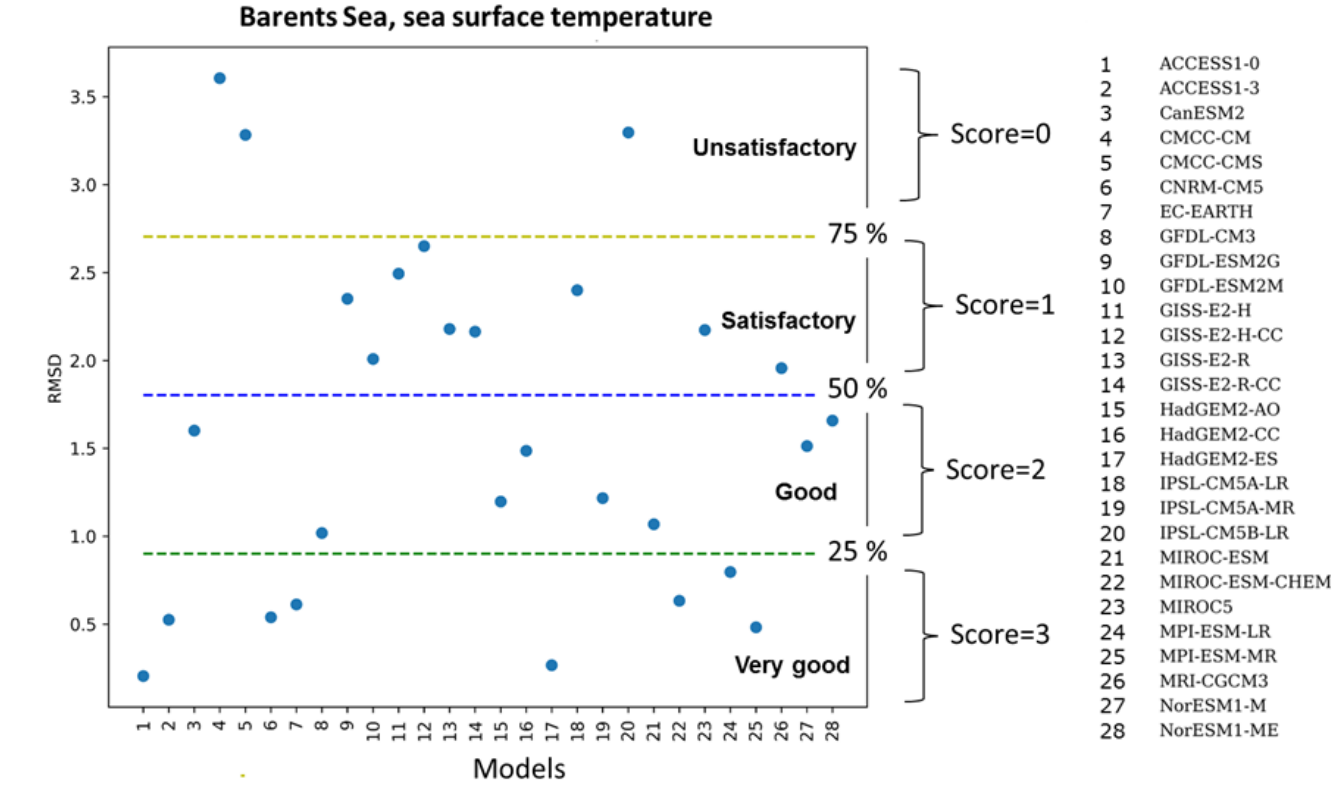

Figure 2: A schematic representation of the percentile score-based model ranking method.

https://doi.org/10.5194/bg-2019-177
Preprint. Discussion started: 3 June 2019

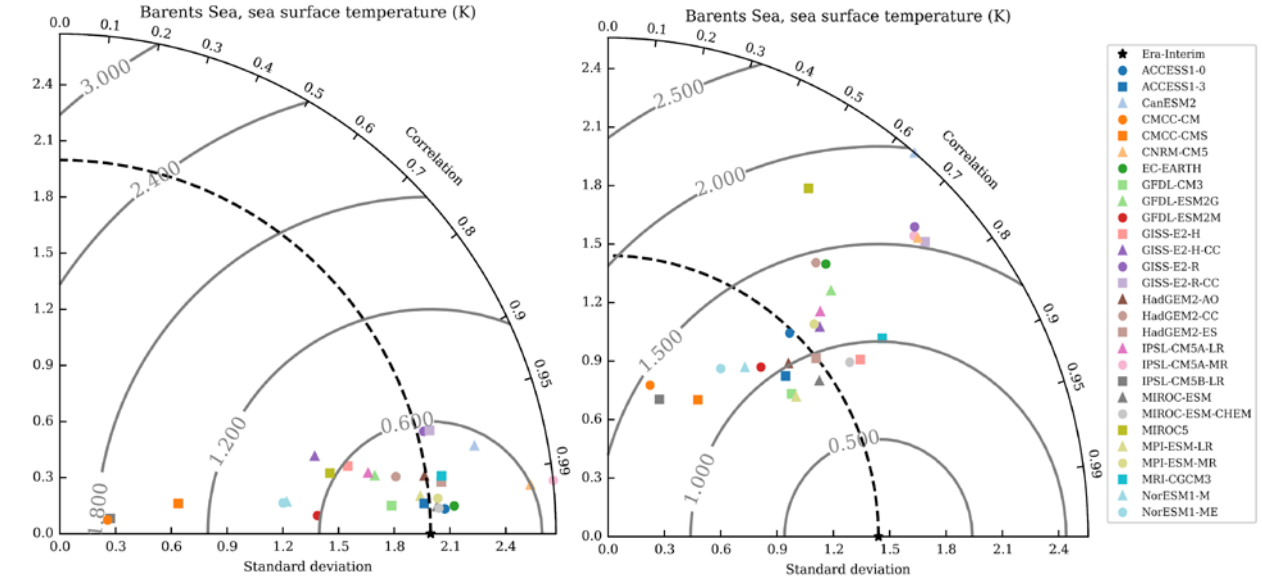

Figure 3: Taylor diagrams for the seasonal cycle (left) and interannual variability (right) of SST in the Barents Sea.

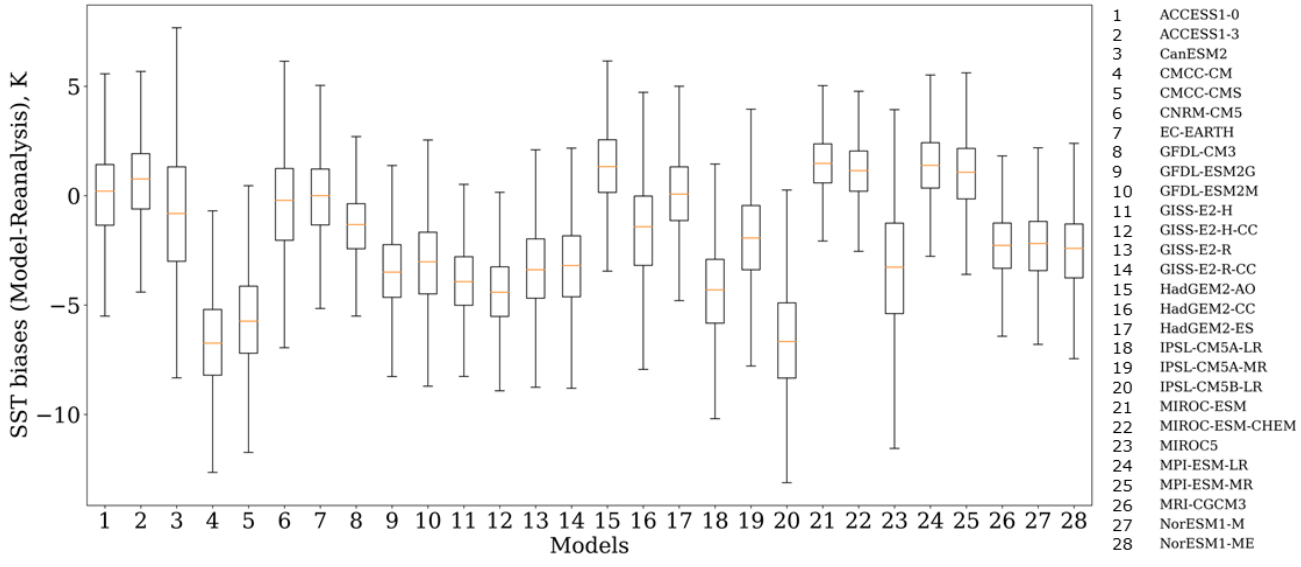

Figure 4: Box plots of spatial distribution of SST biases in the Barents Sea.

https://doi.org/10.5194/bg-2019-177
Preprint. Discussion started: 3 June 2019

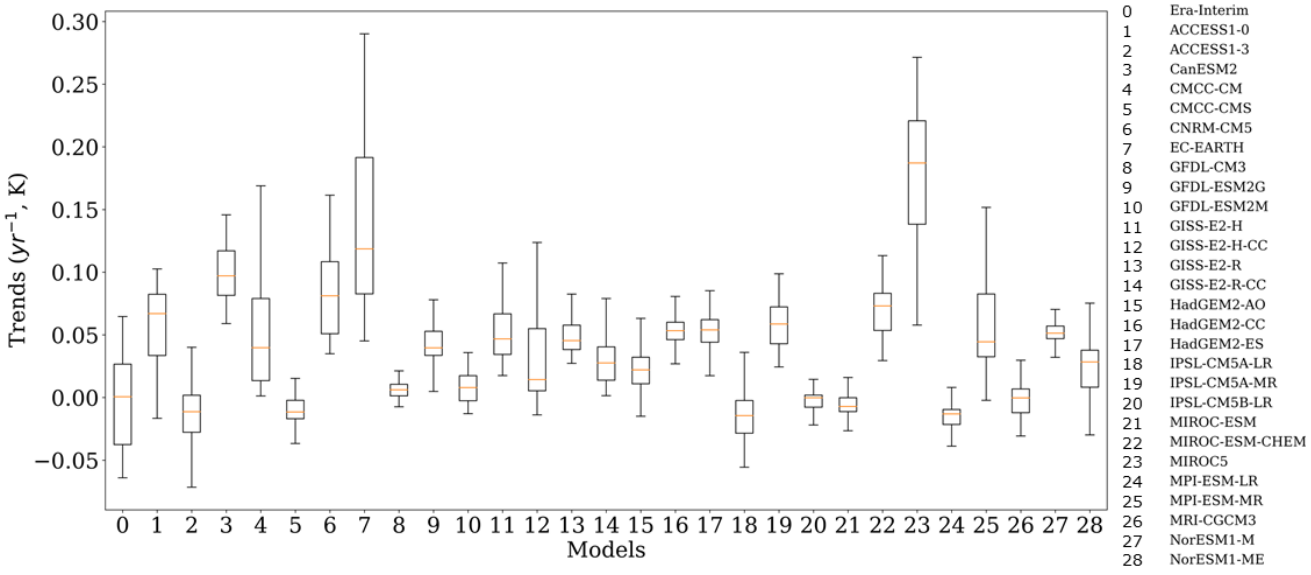

Figure 5: Box plots of spatial distribution of SST trends in the Barents Sea.

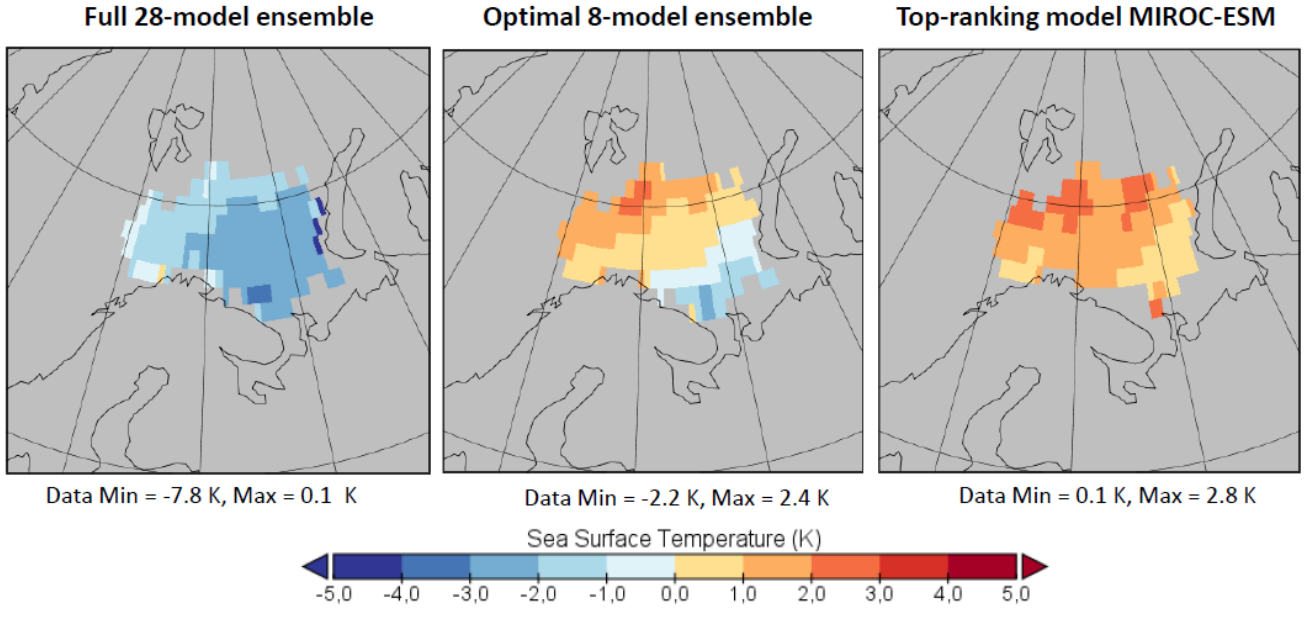

Figure 6: Spatial distribution of biases in SST between models and reanalysis in the bloom area of the Barents Sea for the blooming period.

https://doi.org/10.5194/bg-2019-177
Preprint. Discussion started: 3 June 2019

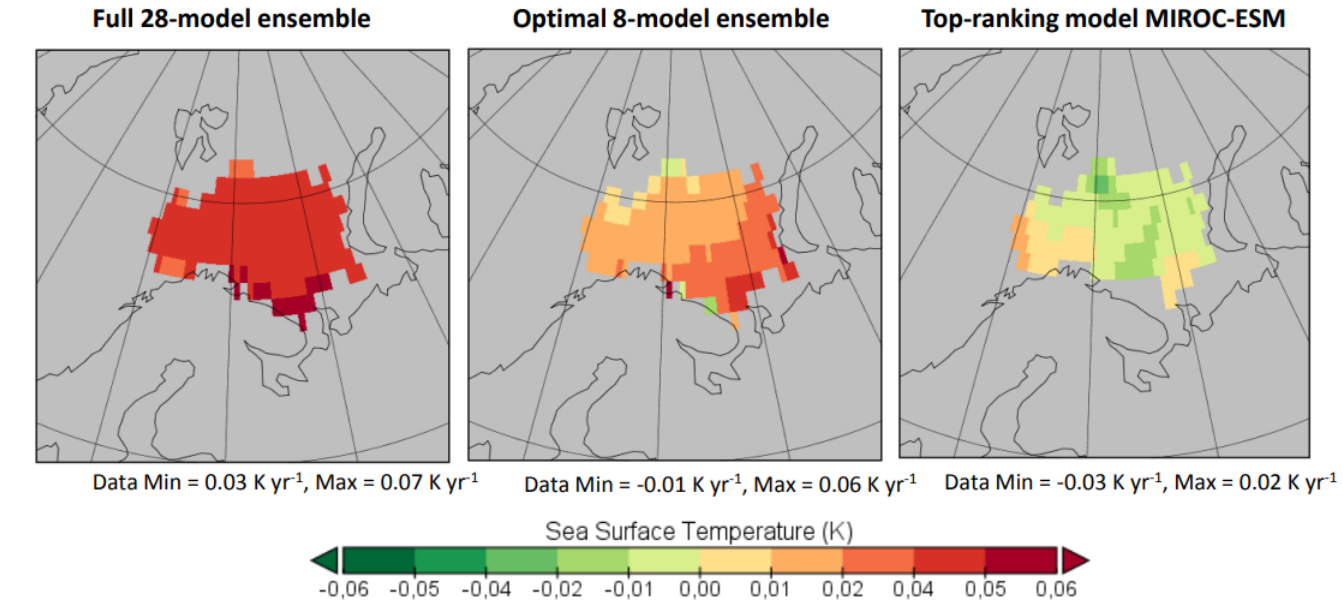

Figure 7: Spatial distribution of errors in annual SST trends (model minus reanalysis) in the bloom area of the Barents Sea for the blooming period

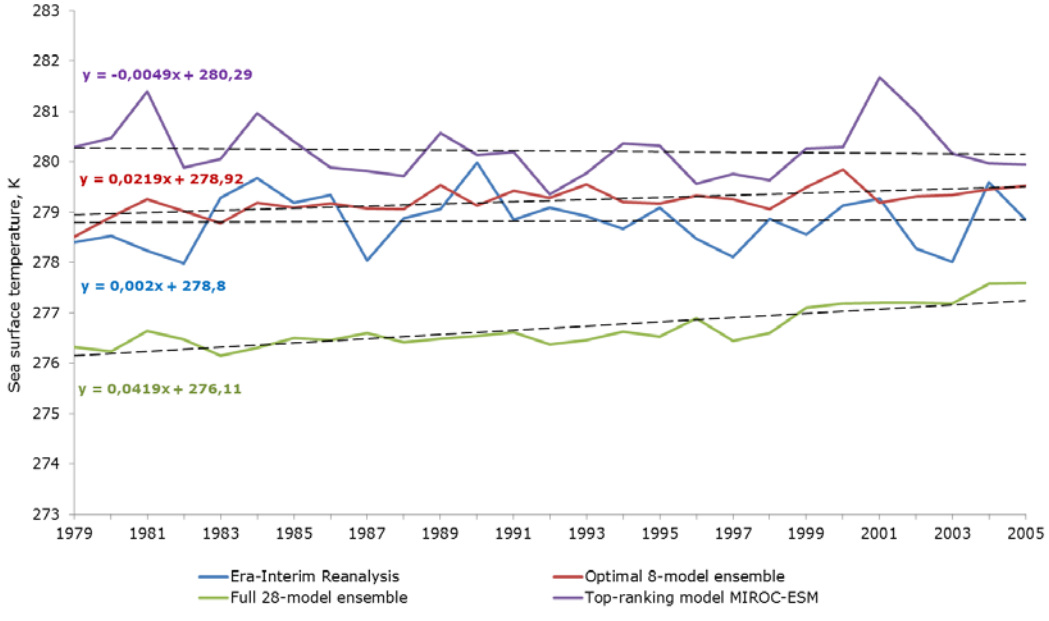

Figure 8: SST variability and trends in the Barents Sea for the blooming period over 1979-2005.

https://doi.org/10.5194/bg-2019-177
Preprint. Discussion started: 3 June 2019

ID	CMIP5 models	Barents Sea					Bering Sea					Greenland Sea					Labrador Sea					North Sea					Norwegian Sea				
		OCS	SSS	SST	WS	SDSR	OCS	SSS	SST	WS	SDSR	OCS	SSS	SST	WS	SDSR	OCS	SSS	SST	WS	SDSR	OCS	SSS	SST	WS	SDSR	OCS	SSS	SST	WS	SDSR
1	ACCESS1-3	**23**	**34**	**33**	28	**27**	30	23	17	27	24	22	**31**	26	**29**	**31**	**27**	29	18	**30**	13	**29**	**30**	32	23	27	23	32	**36**	24	25
2	ACCESS1-0	**26**	**33**	**34**	28	**27**	27	24	26	26	**29**	18	**31**	27	27	**33**	**27**	26	22	26	20	**31**	**30**	30	23	25	**28**	31	**35**	25	24
3	CanESM2	**25**	26	24	**29**		27	24	26	14		19	15	**30**	19		16	29	**33**	9		**26**	22	**34**	18		**29**	22	**35**	21	
4	CMCC-CM	7	26	9	23	21	29	22	25	27	14	21	28	16	27	21	23	**30**	18	20	14	**27**	23	25	24	8	13	**33**	22	**30**	8
5	CMCC-CMS	16	22	14	24	23	29	23	25	28	15	**25**	**33**	**32**	22	16	**25**	**35**	15	21	15	24	19	30	25	13	24	31	**36**	**28**	14
6	CNRM-CM5	18	31	29	28	13	**31**	25	26	30	26	21	**32**	23	26	19	**29**	**30**	**30**	26	**29**	23	**31**	30	**28**	**29**	25	**34**	31	**27**	25
7	CSIRO-Mk3-6-0	20	23		19	21	21	**26**		**31**	14	20	**35**		26	10	21	27		**30**	17	23	25		24	16	19	**33**		15	13
8	EC-EARTH			27					27					**35**					28					30					**36**		
9	FGOALS-g2	17					4					8					24					11					12				
10	GFDL-CM3	20	32	**34**	27	23	**32**	20	**32**	**32**	26	19	30	**32**	21	**28**	**27**	25	25	**28**	**28**	23	19	31	**29**	22	**26**	**33**	**36**	**27**	24
11	GFDL-ESM2G	21	30	23	26	26	29	25	20	30	14	**24**	27	22	**30**	24	20	27	**29**	**27**	21	22	27	32	27	26	**26**	**33**	30	26	25
12	GFDL-ESM2M	15	**33**	26	27	25	**32**	20	24	29	20	**23**	**33**	23	23	18	**27**	**32**	24	**27**	**27**	24	18	29	**28**	28	25	**33**	33	23	27
13	GISS-E2-H	10	29	25	**29**	12	26	19	29	30	**28**	16	**32**	28	**28**	25	15	15	14	19	**28**	20	**30**	32	**28**	**31**	17	**33**	**36**	19	**34**
14	GISS-E2-H-CC	14	24	24	**30**	12	25	21	**32**	**32**	26	13	24	25	**28**	17	18	23	23	18	19	19	**31**	32	26	**29**	20	27	**35**	26	**32**
15	GISS-E2-R	19	8	20	26	12	28	25	25	**32**	**29**	**25**	29	28	**30**	22	22	26	27	26	**29**	23	28	31	**29**	**30**	23	32	33	**27**	**34**
16	GISS-E2-R-CC	20	9	22	27	11	29	**27**	28	**32**	**30**	**24**	28	26	**30**	25	22	22	**30**	**28**	**28**	22	25	30	**30**	**29**	24	**35**	29	**27**	29
17	HadCM3				16					28					25					**27**					27					19	
18	HadGEM2-AO	**26**	32	31	**30**	**29**	30	**28**	29	**32**	**30**	17	23	27	**31**	**33**	19	11	**30**	**28**	13	**28**	**30**	**35**	20	28	**26**	31	34	21	**31**
19	HadGEM2-CC	**22**	32	25	**30**	25	29	**26**	**32**	30	**29**	20	19	**31**	**29**	**33**	22	20	**30**	**30**	16	**29**	**31**	**33**	**28**	**31**	**27**	32	**35**	25	**32**
20	HadGEM2-ES	21	**33**	**33**	27	**30**	25	24	28	30	27	17	25	28	**28**	**33**	25	17	26	**29**	13	**28**	26	32	**29**	**30**	**28**	30	33	23	**32**
21	INMCM4				**30**	**32**				26	**32**				16	**33**				18	**30**				23	**31**				24	28
22	IPSL-CM5A-LR	18	12	22	23	**29**	30	25	**34**	27	26	18	29	25	19	25	19	**31**	23	24	26	22	12	21	13	20	17	29	28	17	25
23	IPSL-CM5A-MR	20	18	23	24	**29**	**33**	22	**32**	**31**	24	17	28	**32**	27	**27**	21	27	25	24	23	25	7	26	23	28	25	31	31	18	27
24	IPSL-CM5B-LR	11	9	11	15	**27**	**33**	**27**	22	**31**	26	15	11	12	18	13	14	21	**31**	23	19	21	13	18	14	16	12	13	25	14	22
25	MIROC4h				**32**					18					**28**					21					27					**28**	
26	MIROC5		31	14	28	22		14	16	24	**31**		**32**	**33**	28	**32**		**31**	19	21	**27**		25	20	**28**	25		24	17	25	**32**
27	MIROC-ESM		31	**35**	15	26		13	**31**	**33**	20		29	22	26	20		**30**	**29**	26	9		26	**34**	16	13		30	34	16	25
28	MIROC-ESM-CHEM		30	**34**	19	23		15	**31**	**31**	21		29	20	25	18		**34**	28	21	10		28	**34**	15	18		28	33	16	25
29	MPI-ESM-LR	21	31	**34**	25	21	**32**	**29**	24	**31**	11	12	**33**	29	21	19	16	22	21	21	10	**26**	**31**	**33**	27	19	13	31	34	**28**	23
30	MPI-ESM-MR	17	**33**	**32**	24	19	**31**	**28**	21	29	15	17	**31**	**31**	25	18	12	24	28	20	15	23	**31**	**35**	25	18	13	25	**35**	**27**	23
31	MRI-CGCM3	**26**	20	27	13	25	28	**28**	**30**	10	26	**26**	13	25	16	19	21	16	26	14	18	20	29	32	12	28	**28**	20	33	15	**33**
32	MRI-ESM1				12					9					11					14					8					16	
33	NorESM1-M		**33**	25		20		17	24		13		30	26		10		23	23		14		**30**	**34**		25		31	33		25
34	NorESM1-ME	**23**	**33**	27		23	28	23	23		15	**23**	**31**	20		14	**27**	21	28		10	25	**30**	31		28	24	**35**	32		23
	total selected models	7	7	8	7	8	7	8	8	11	8	7	11	8	10	9	7	8	8	10	8	8	11	8	9	8	8	9	10	9	8

30 - selected optimal model ensemble

- score < 25% "very good"

- 25% < score < 75% "good" & "satisfactory"

- score > 75% "unsatisfactory"

Figure 9: Heat map with the final model scores obtained using the percentile score-based model ranking method for five forcing factors (sea surface temperature (SST) and salinity averaged over 0-30 m (SSS), surface wind speed at 10 m (WS), ocean surface current speed (OCS), and shortwave downwelling solar radiation (SDSR) for the Barents, Bering, Greenland, Labrador, North, and Norwegian seas.